

GHz sandwich strip inductors based on Fe/N bilayers

A. Gromov, V. Korenivski, and D. Haviland

23rd March 2024

Nanostructure Physics, Royal Institute of Technology, 10044 Stockholm, Sweden.

Abstract

Planar strip inductors consisting of two Fe/N bilayers enclosing a conducting bilayer made of Cu, were fabricated on oxidized Si substrates. The inductors were 1 mm long, 2 to 100 μm wide, with layers of thickness 0.1 μm for the magnetic bilayers and 0.5 μm for the conductor. The soft ($H_c = 4 - 80 \text{ Oe}$) magnetic layers were biased during impedance measurement by applying an external field along the strip length thereby facilitating the transverse susceptibility configuration. Biased strips exhibited 70 to 100% inductance enhancement at 1 GHz with quality factors $Q = 4.5$ to 3, respectively. The magnetic contribution to the total flux in the narrow devices was less than predicted theoretically, which was attributed to hardening of the magnetic material at the edges of the strip, where the deposition was close to 60 incidence. Test bilayers were fabricated on tilted substrates and found to develop a very high anisotropy (up to 1 kOe) for deposition angles larger than 30°. Optimizing the flux closure at the strip edges and using thicker conductor layers is essential for further improving the performance of sandwich strip inductors.

1 Introduction

There have been numerous efforts to enhance the performance and diminish the size of planar inductors for sub-GHz applications by using magnetic films. Several recent reports extended these efforts to 1-2 GHz by studying magnetically enhanced spirals and strip inductors. A magnetically clad spiral showed 10-20% inductance enhancement [1]. An inductance gain of 70% was observed at 1 GHz for a magnetic sandwich strip, though with $Q < 1$ [3]. The inductor is a fundamental electronic component, which is least compatible with silicon integration. Achieving high specific inductance values is crucial for miniaturization of inductors used in filters, oscillators, matching networks, etc., in high frequency integrated circuits. The status of research in the field has recently been reviewed [2]. A GHz magnetic inductor having a substantial inductance gain (preferably more than a factor of 2) over the corresponding air-core design and acceptable efficiency ($Q > 3$) at ~1 GHz has not yet been demonstrated. We report on the fabrication of magnetic/conductor sandwich strip inductors using Fe-N films. The inductors exhibit a 2-fold inductance gain with $Q > 3$ at 1 GHz, a substantially better performance than reported previously. We analyze the factors limiting the magnetic efficiency and high frequency performance of these devices.

2 Sample preparation and measurements

The inductors are strips of length 1.15 mm with width varying from 2 to 100 μm . The inductors were fabricated on oxidized Si substrates (1 μm thick oxide layer) with a lift-off process. A two layer resist system consisting of a low contrast bottom layer (PMGI) and a high contrast top layer (ZEP) was used. The pattern was defined using an e-beam writer. The mask was developed to have an undercut of 0.5-1.5 μm , as shown schematically in Fig. 1. The following deposition sequence was used: sputtering 0.1 μm of FeN, evaporating 0.5 μm of Cu, sputtering 0.1 μm of FeN. A 5 nm thick capping layer of gold was evaporated to ensure a good contact for impedance measurements. Magnetic material covering the edges of the strips (angles) was achieved by utilizing the difference in shadow depth for sputtering of the magnetic layers (dashed arrows) and evaporation of the

conductor (solid arrows). A magnetic/conductor/magnetic sandwich with magnetic flux closure at the edges is thus obtained with one lift-off mask.

The Fe-N was produced by reactive sputtering from an Fe target using an argon/nitrogen gas mixture with typically 4% partial pressure of nitrogen (p_N). The sputtering pressure used was 3 mTorr and the rate was 4.8 Å/s. Thus sputtered, the Fe-N material had a resistivity of 40 mΩ/cm as measured using a four-point technique. Vibrating sample magnetometer (VSM) measurements show a square loop with coercivity $H_c = 4.8$ Oe, saturation magnetization $4 M_s = 17$ kGs, and essentially no in-plane anisotropy. The copper film was evaporated at 10 Å/s and showed the resistivity of 2.4 mΩ/cm. The depositions were made at ambient temperature.

An HP 8714C network analyzer with a Cascade 12 GHz fixed-pitch probe was used for impedance measurements. The real and imaginary parts of the impedance were obtained from reflection measurements in the 30 MHz–3 GHz frequency range. The following de-embedding procedure was used. The network analyzer was calibrated to the probe plane. A correction was made for the electrical delay corresponding to the probe length. The contact resistance was evaluated from the low frequency limit for various device geometries. The resistance scaled linearly versus the inverse strip width with a 0.24 Ω offset, which was attributed to contact resistance. The Cascade probe introduces a series impedance, which was determined using Cu test strips of varying width. The impedance of these strips could be accurately modeled and compared with measurements. The parallel impedance due to the measurement configuration was found to be negligible for strip widths greater than 2 μm.

3 Results and discussion

The inductance, $L = \text{Im}(Z)/\omega$, is plotted in Fig. 2 as a function of frequency for different inductor widths. The magnetic films have no preferred in-plane orientation of the magnetization. The weak, if any, in-plane anisotropy can result in an arbitrary in-plane orientation of the magnetic moments (domains) in the films when no biasing field is applied. This would diminish the magnetic response and limit the frequency range of these devices, as observed (dashed lines, Fig. 2). To avoid these undesirable effects, we biased the films in an external magnetic field parallel to the strip length. In the

biased case, we observe a flat response out to the ferromagnetic resonance (FMR) cutoff (Fig. 2, solid lines). In what follows, we will discuss only the biased response.

3.1 Magnetic reluctance analysis

From the low frequency limit of the inductance (Fig. 2, solid lines) we can determine the magnetic contribution, which excludes any dissipation or resonance effects at high frequencies. The total inductance in this limit, $L = L_0 + L_m$, is the sum of the air-core inductance of the strip, L_0 , and the contribution due to the magnetic film, L_m . In Fig. 4, L_m is plotted versus the strip width. The experimental data deviate from the ideal $1/w$ width (dash-dotted line) behavior expected when there is perfect magnetic flux closure at the edges. The observed magnetic contribution to the inductance is below the theoretical value for narrow strips, while it approaches the expected values for wide strips. This behavior indicates an incomplete flux closure at the edges, which plays a progressively larger role as the width of the strip is reduced [4].

In order to gain insight into the magnetic state of the angle we model the data in Fig. 3 using the theory of Ref. [4] for three different cross sectional geometries: a angled edge, no-angle, and a three section arbitrary edge-gap. In the case of the open structure (no angles, dashed line, Fig. 3) the relative permeability is the only fitting parameter. The fit is poor, indicating that some flux closure at the edges does take place. Fig. 4a is a SEM image of the inductor edge showing that the magnetic film becomes thinner and possibly is discontinuous towards the very edge sloped at approximately 60° . This edge geometry is indeed an intermediate case between perfect flux closure and no flux closure. To model this case we use a model geometry depicted in Fig. 4b [4]. Assuming the angle width is the same as the thickness of the magnetic films and assuming the films and angle have the same permeability, we fit the width dependence of the inductance by introducing a angle gap. A good fit of the experimental data is obtained for $\mu_r = 390$ and the angle gap of $g = 44\text{nm}$. It should be noted that the effect on the inductance of introducing a gap in the angle is similar to the effect of a reduced permeability of a continuous angle. In any case, our data clearly exhibit an incomplete flux closure at the edges.

3.2 Magnetic properties of the angle

Because the cross section of the sandwich does not appear to have any gap, we suspect that poor flux closure is actually due to lower permeability of the angle. To investigate this effect, we varied the angle of the substrate with respect to the source during the evaporation of the conductor through the lift-off mask. In this way we can vary the slope of the conductor edge between approximately $\theta = 45^\circ$ and 80° . Fig. 4a is a SEM image of the inductor cross-section showing that the magnetic film towards the very edge is sloped at approximately 60° to the strip's plane and becomes slightly thinner. For the top film deposition the incident flux of Fe-N is perpendicular to the Cu surface except at the edges, where the angle of incidence is in this case 60° . Deposition of soft magnetic materials, including Fe-N, on tilted substrates is known to result in a strong magnetic anisotropy perpendicular to the direction of incidence [5]–[7]. In addition, films deposited at large oblique angles are typically thinner. In order to quantify the magnetic state at the edge, we have fabricated test Fe-N films sputtered directly on oxidized Si at 0° to 60° angle of incidence. The results of VSM measurements for these films are shown in Fig. 5. The normal incidence films show no preferred in-plane orientation of the magnetization. The films deposited at 20° incidence develop a weak in-plane anisotropy. The easy-axis coercivity, H_{ce} , increases while that for the hard axis, H_{ch} , decreases, and a uniaxial anisotropy with $H_k \approx 100$ e appears. The films sputtered at $\theta = 60^\circ$ (inset) show $H_{ce} \approx 2000$ e and $H_k \approx 4000$ e. For the films sputtered at $\theta = 4^\circ$ – 8° , H_{ce} is the same, while anisotropy increases up to $H_k = 600$ – 8000 e. Increasing the angle to the 80° , we obtain for $H_k = 0.9$ – 1 kOe. This growth induced anisotropy is directed along the length of the strip, leading to more than an order of magnitude reduction in the transverse permeability, and thus degrading the inductive response of the film. Two possible mechanisms for this anisotropy are discussed in the literature (see, e.g., [7]). The first is the shape anisotropy of elliptical magnetic columns that are typically present in films deposited at oblique angles due to the self-shadowing effect [6, 5]. This effect has recently been analyzed in detail for Co films on underlayers deposited at oblique angles [8] and was shown to result in up to 1 kOe of anisotropy. Another possible origin of the oblique-growth induced anisotropy in magnetic films discussed in the literature is due to magnetostriction. Although we have not performed independent measurements of the stress in our films as a

function of the incidence angle, the amount of stress needed to produce such high anisotropy values appears unreasonable if one takes typical values for the magnetostriction of Fe-N.

In order to directly verify the effect of the angle on the inductance we have fabricated two inductor sets under identical conditions, varying only the Cu edge angle, $\theta = 45^\circ$ and 80° . The magnetic contribution to the total inductance is shown in Fig. 6. The difference in L_m for the two inductor sets increases for small widths, approaching 25% for the 5 μ m wide strip. We attribute this increase in L_m to a magnetically softer angle in the 45° -edge inductor, resulting in a better flux closure.

3.3 HF performance

The contribution of the angles to the magnetic inductance becomes smaller as the width of the strip is increased (see Fig. 3). The measured inductance of the 50 μ m wide strip is essentially the value expected for a sandwich with perfect flux closure, hence the model for the impedance of a closed magnetic structure should apply (see Appendix and [9]). The inductance and quality factor for the 50 μ m width strip measured in three biasing fields are shown as functions of frequency in Fig. 7a and 7b, respectively, along with the theoretically fitted curves. Fixing the geometrical parameters at the measured values, a good fit can be obtained by varying the permeability and intrinsic damping. If we use the same parameters to fit the impedance of the 10 μ m strip, the deviation from the predicted performance is significant (see Fig. 8). In order to obtain a good fit not only the permeability has to be significantly reduced (by roughly a factor of two) but the dissipation constant has to be significantly increased: from $\alpha = 0.028$ (consistent with values 0.020-0.025 measured on test films) to 0.06. The reduction in the effective permeability for narrow strips can be attributed to the increasing influence of incomplete flux closures at the edges. However, the increase in the damping constant is not expected to depend on the width of the strip in the simplest picture. A probable cause of the increased dissipation is that an increasing portion of the magnetic flux leaks through the conductor near the angle, causing screening currents in the conductor. This dissipation mechanism is not accounted for in the 'closed-flux' model [9] but known to be the dominating loss mechanism in sandwiches without flux closure [10].

The inductance and quality factor at 1 GHz are shown in Fig. 9 as a

function of the inductor width. A 2-fold inductance gain with $Q \approx 3$ was obtained for the 20 μm wide inductor. By varying the width of the device the inductance gain can be compromised for higher quality factor.

4 Conclusions

We have demonstrated a significant specific inductance gain at 1 GHz by using magnetic/conductor sandwiches. Several issues should be addressed for further improving the device performance. The use of soft μm s with resistivities in excess of 100 $\mu\Omega/\square$ should allow thicker magnetic layers in the sandwich, resulting in larger magnetic flux and therefore larger inductance, without increasing dissipation. Use of thicker conductor layers should yield higher quality factors, provided the edge flux closures are not thereby degraded. Control of the properties of the magnetic μm s at the strip edges to achieve efficient flux closure is crucial for both improving the inductance gain and quality factor in the GHz range. Inducing a longitudinal in-plane anisotropy in the μm s, for example by field annealing, should eliminate the need for external biasing.

5 Appendix

Here we reduce the full solution for the impedance of a 'closed' sandwich inductor [9] to a simple expression, which should be useful in analyzing or designing sandwich inductors without insulation layers. Regrouping the impedance from [9] in such a way as to separate the contribution of the conductor one obtains:

$$Z(\omega) = \frac{1}{w(b_0 + 2d_1)} + i\omega \frac{d_0}{2} \ln \frac{2d_0}{w} + 1 + i\omega \frac{1}{2w(1+i)} \tanh \left((1+i) \frac{d_1}{\delta_1} \right) k(\omega)$$

where $\delta_{0(1)} = \sqrt{\frac{2}{\omega \mu_0(1) \sigma_{0(1)}}}$ is the skin depth in region '0' ('1'). The first term here is due to the parallel connection of the conductor and magnetic μm resistances, $R_0 = \frac{R_c R_m}{R_c + R_m}$. The second term is the air-core reactance $i\omega L_0$. The last term represents the magnetic contribution, including the

skin effect. The complex coefficient,

$$k(\omega) = \frac{\frac{1}{b_0} \tanh\left((1+i)\frac{b}{2d_0}\right) + \coth\left((1+i)\frac{d}{d_1}\right)}{\frac{1}{b_0} \tanh\left((1+i)\frac{b}{2d_0}\right) + \tanh\left((1+i)\frac{d}{d_1}\right)} \frac{\coth\left((1+i)\frac{d}{d_1}\right)}{(1+i)\frac{d}{d_1} + 1 + \frac{b_0}{2d_1}}$$

is the correction factor arising from the current redistribution between the conductor and magnetic layers. When $d < b$; $b_1 \rightarrow 0$, k becomes very close to unity, and the largest error introduced by omitting this coefficient is less than $\frac{2d_1}{b_0}$, which is small at all frequencies. Thus, we can express the impedance using the equivalent circuit of Fig. 10 as

$$Z(\omega) = R_0 + i\omega L_0 + i\omega L_m(\omega);$$

where

$$R_0 = \frac{R_c R_m}{R_c + R_m} = \frac{1}{w(b_0 + 2d_1)};$$

$$L_0 = \frac{b_0}{2} \ln \frac{2}{w} + \frac{1}{2}$$

is the exact air-core inductance [11] differing by 10% from the approximation used in [9], and

$$L_m(\omega) = \frac{1}{2w(1+i)} \tanh\left((1+i)\frac{d}{d_1}\right)$$

is the inductance of a magnetic film in a uniform magnetic field [12]. The effective slab thickness is $2d$, which at first glance might appear counter intuitive, but is a natural result of current redistribution in a sandwich with the layers in direct electrical contact. The intrinsic transverse permeability μ_1 is the well known Landau-Lifshitz permeability (see, e.g., [13]):

$$\mu_1 = \frac{(\mu_H + \mu_M)^2 - \mu^2}{\mu_H (\mu_H + \mu_M) - \mu^2}; \quad (1)$$

$$\mu_M = 4 M_s; \quad \mu_H = (H_0 + H_K) - i\omega; \quad (2)$$

where γ is the gyromagnetic ratio, α - phenomenological damping parameter, M_s - saturation magnetization, H_K - uniaxial anisotropy field in z-direction, and H_0 - external uniform magnetic field.

References

- [1] M . Yam aguchi, K . Suezawa, Y . Takahashi, K . I. Arai, S. K ikuchi, Y . Shim ada, S. Tanabe, K . Ito, J. M agn. M agn. M ater., 215-216, 807, 2000.
- [2] V . K orenivski, J. M agn. M agn. M ater. 215-216 (2000) 800.
- [3] T . Saito, K . T sutsui, S. Yahagi, Y . M atsukura, H . Endoh, T . E shita, and K . H ikosaka, IEEE Trans. M agn., 35 (5), 3187, 1999.
- [4] V . K orenivski and R . B . van D over, J. A ppl. Phys., 82 (10), 5247, 1997.
- [5] K . O zawa, T . Yanada, H . M asuya, M . Sato, S. Ishio, and M . Takahashi, J. M agn. M agn. M ater., 35, 289, 1983.
- [6] S. Jo, Y . Choi, and S. Ryu, IEEE Trans. M agn., 33 (5), 3634, 1997.
- [7] T . J. K lem mer, K . A . Ellis, L. H . Chen, R . B . van D over, and S. Jin, J. A ppl. Phys., 87 (2), 830 , 2000.
- [8] R . D . M cM ichael, C . G . Lee, J. E . Bonevich, P . J. Chen, W . M iller, and W . F. Egelho , Jr, J. A ppl. Phys. 89 (2000) 5296.
- [9] A . G rom ov, V . K orenivski, D H aviland, R . B . van D over, J. A ppl. Phys., 85 (8), 5202, 1999.
- [10] A . Sukstanskii, V . K orenivski, and A . G rom ov, J. A ppl. Phys. 89 (2001) 775.
- [11] Inductance calculations: working formulas and tables, Frederick W . G rover, New York: Van Nostrand, 1946.
- [12] E . van de R iet and F . Roozeboom , J. A ppl. Phys., 81 (1), 350, 1997.
- [13] N . A . U sov, A . S. Antonov and A . N . Lagarkov, J. M agn. M agn. M ater., 185, 159, 1998.

Figure captions:

- Fig.1. Schematic of the fabrication process.
- Fig.2. Inductance as a function of frequency for 5, 10, 20, 50, and 100 μm wide strips with $H_{\text{bias}} = 0$ (dashed lines) and $H_{\text{bias}} = 350 \text{ e}$ (solid lines).
- Fig.3. The magnetic contribution to inductance, L_m . The expected inductance of a 'closed' magnetic structure (dash-dot line) and an 'open' structure (dashed line).
- Fig.4. Cross-sectional view of the sandwich inductor (a). Modeling geometry (b): μ_0 , t_m - magnetic film thickness, $w_f = t_m$ - finger width, g - gap.
- Fig.5. Hard and easy axis $M-H$ curves for Fe-Ni films deposited at different oblique angles.
- Fig.6. Magnetic inductance versus width for two sets of inductors having the conductor edge angle of approximately $\theta = 45^\circ$ and 80° degrees to the film normal.
- Fig.7. L (a) and Q (b) versus frequency for a 50 μm wide inductor in three biasing fields. Solid lines are theoretical fits using the 'closed' model [9].
- Fig.8. L (a) and Q (b) versus frequency for a 10 μm wide inductor in two biasing fields. Solid lines are theoretical fits using [9] with the parameters from Fig. 7. Dashed lines are fits assuming a reduced permeability and increased damping constant (see text).
- Fig.9. Inductance and quality factor at 1 GHz versus inductor width.
- Fig.10. An equivalent circuit of a magnetic sandwich inductor without insulation layers.

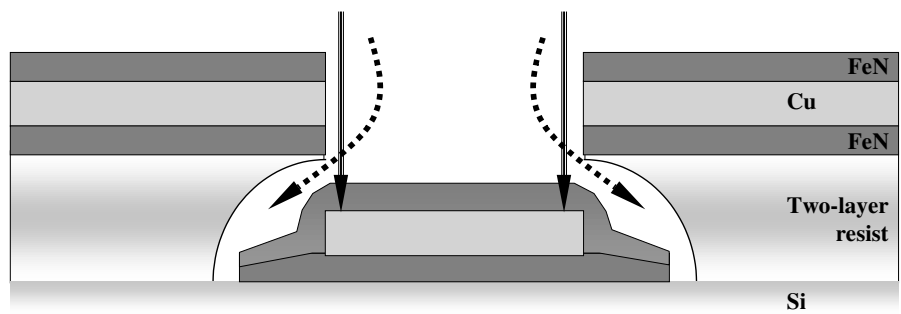


Figure 1: -

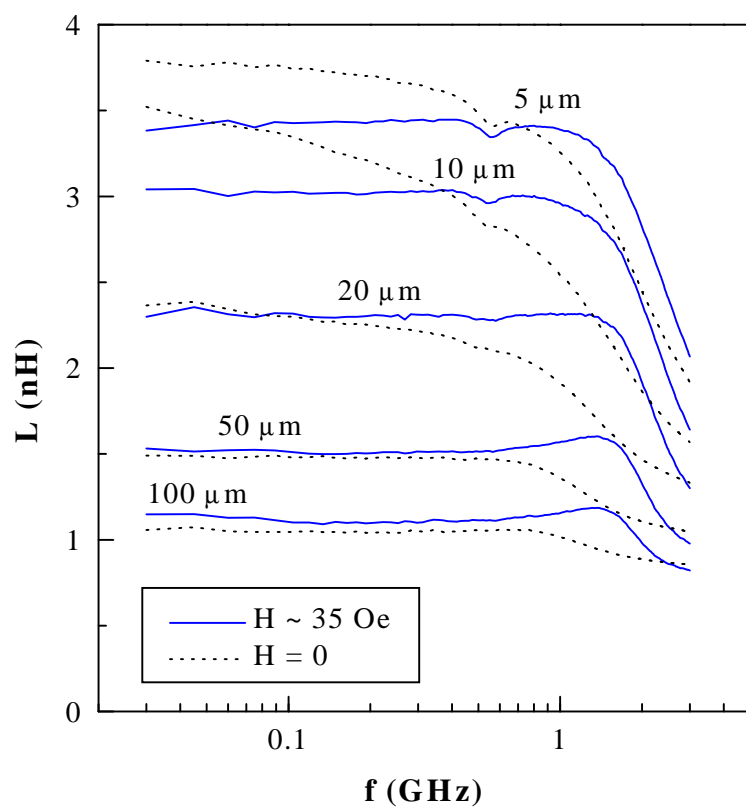


Figure 2: -

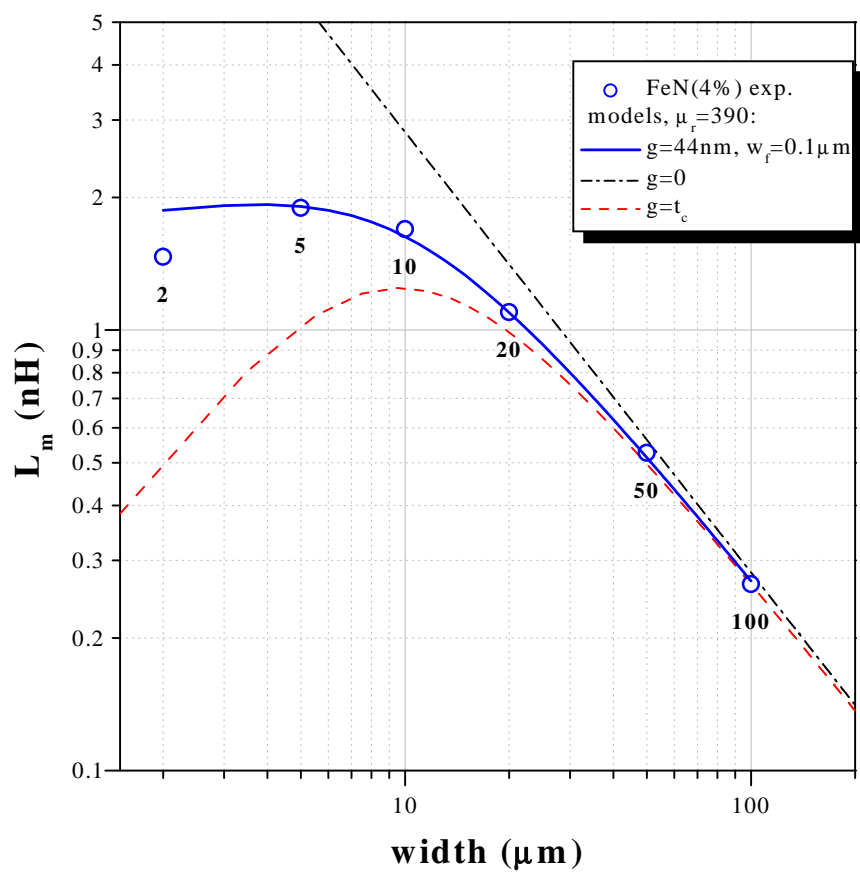


Figure 3: -

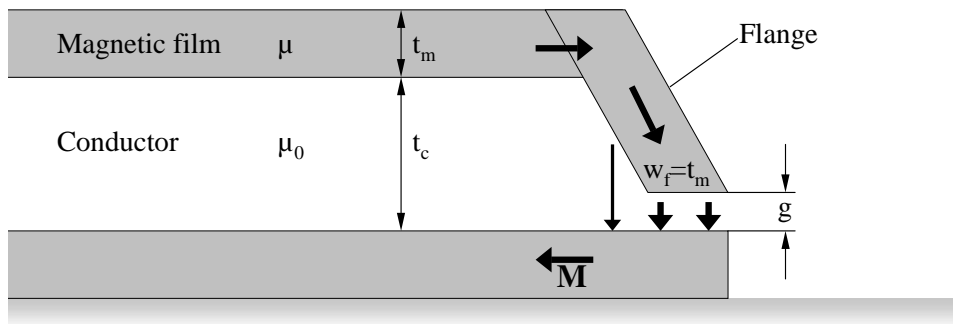
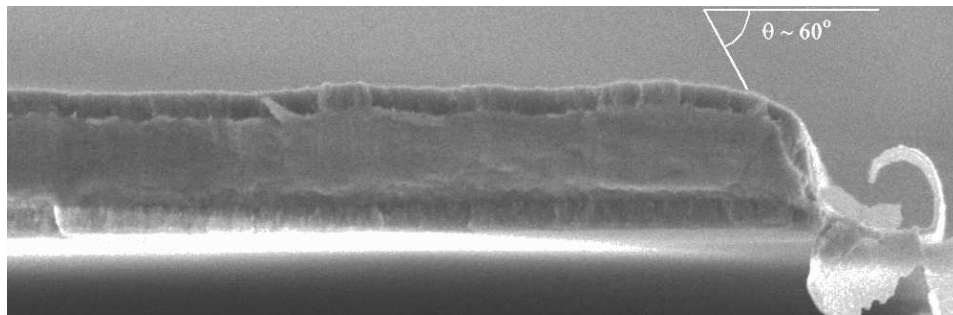


Figure 4: -

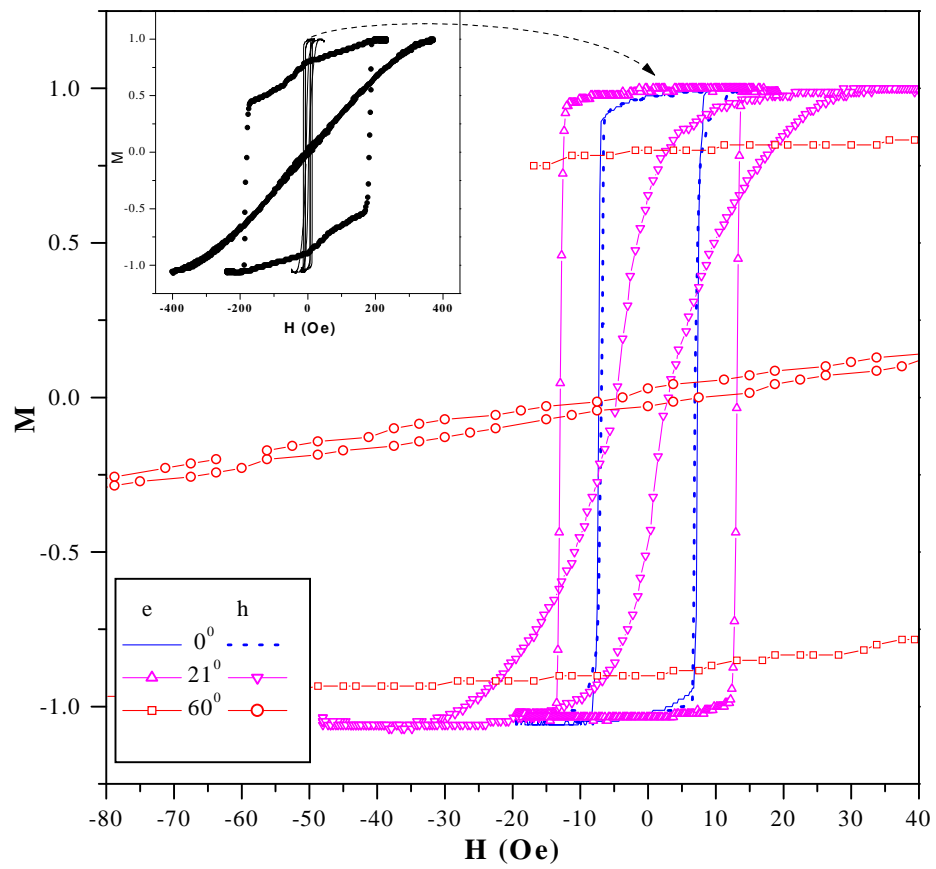


Figure 5: –

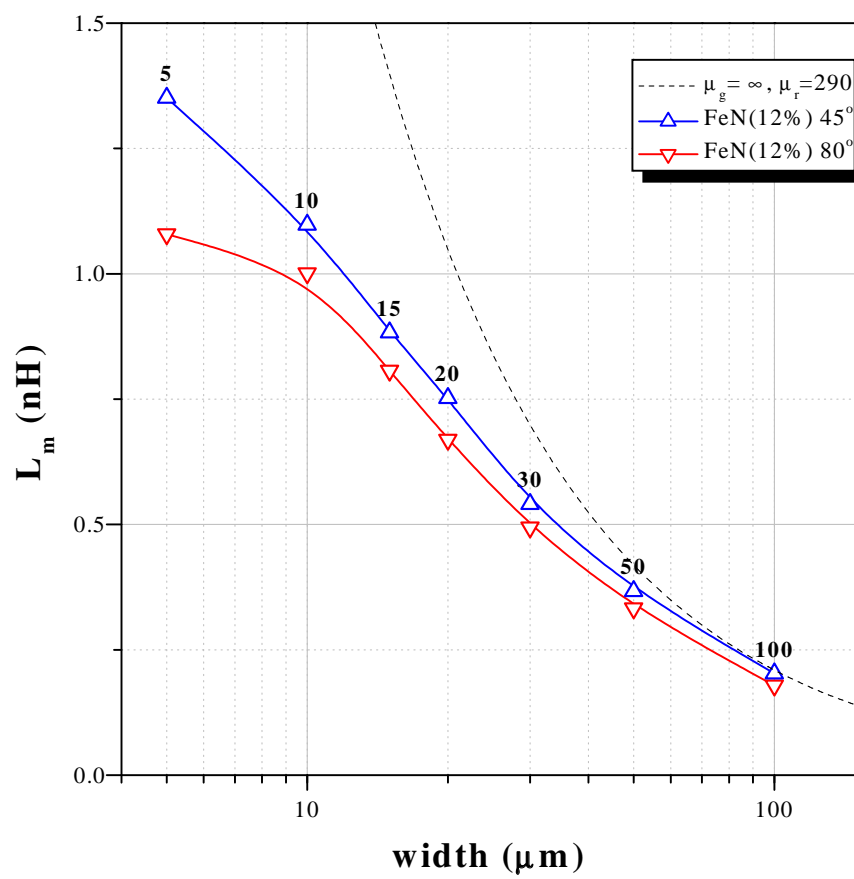
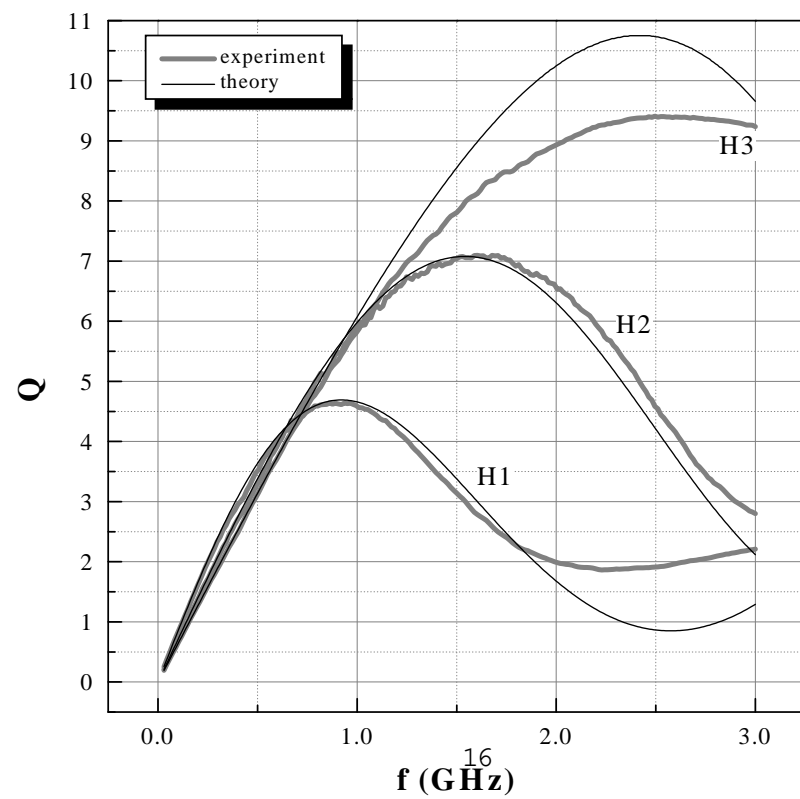
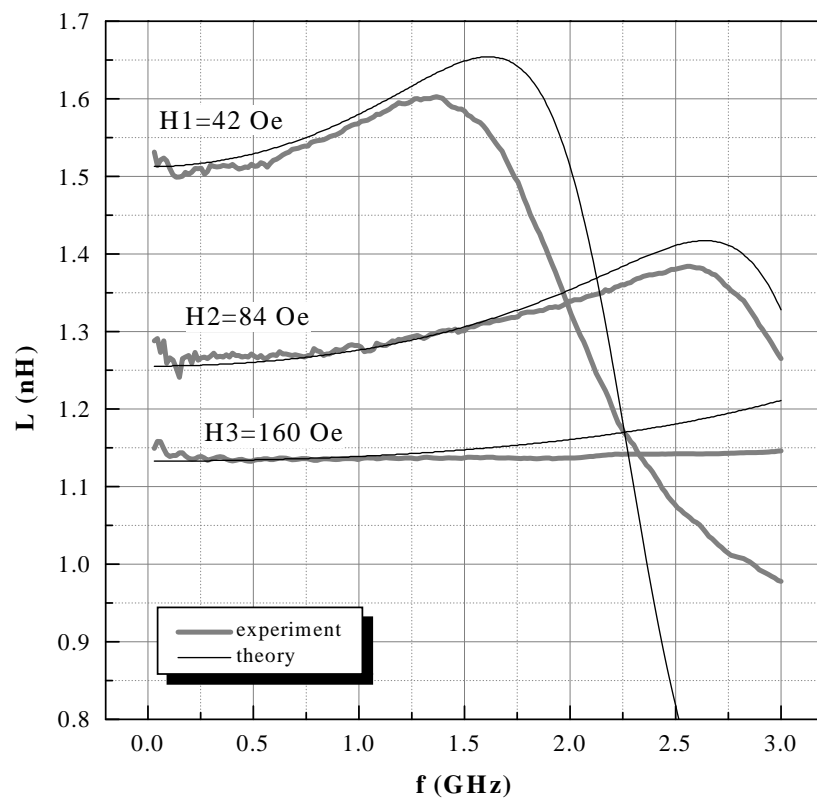


Figure 6: -



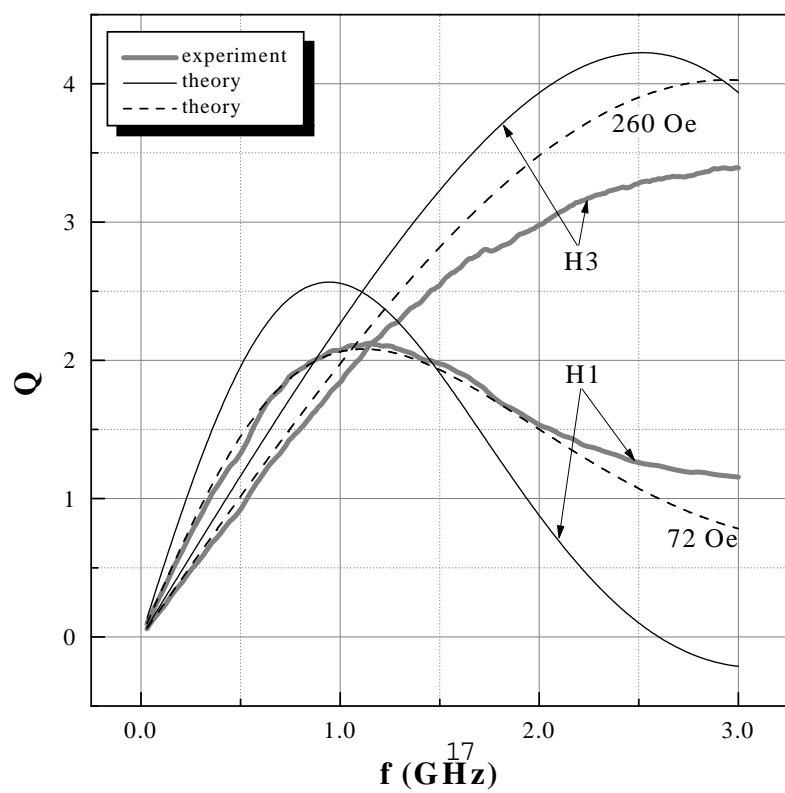
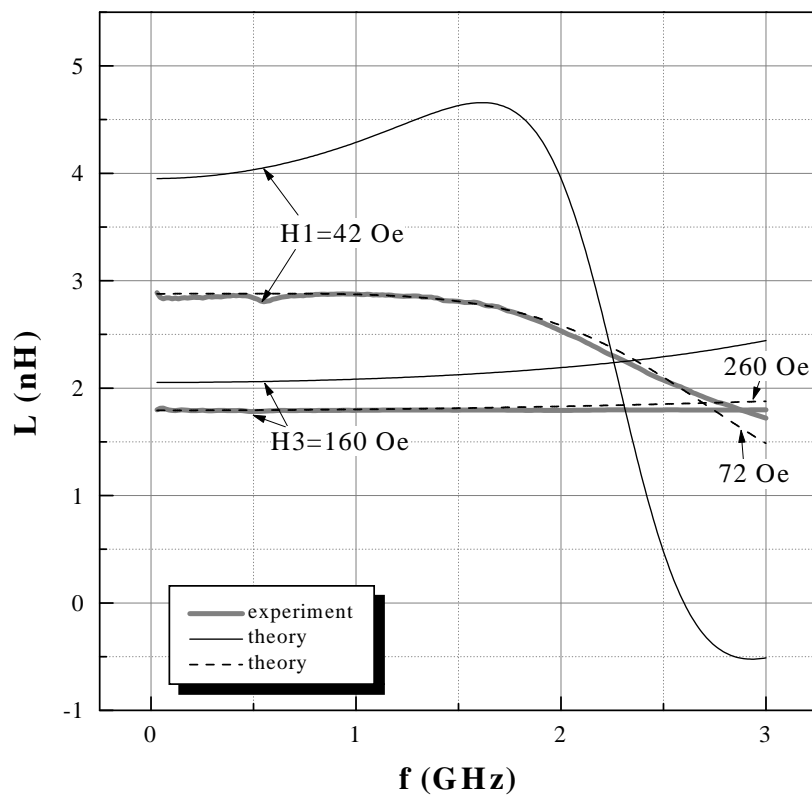


Figure 2

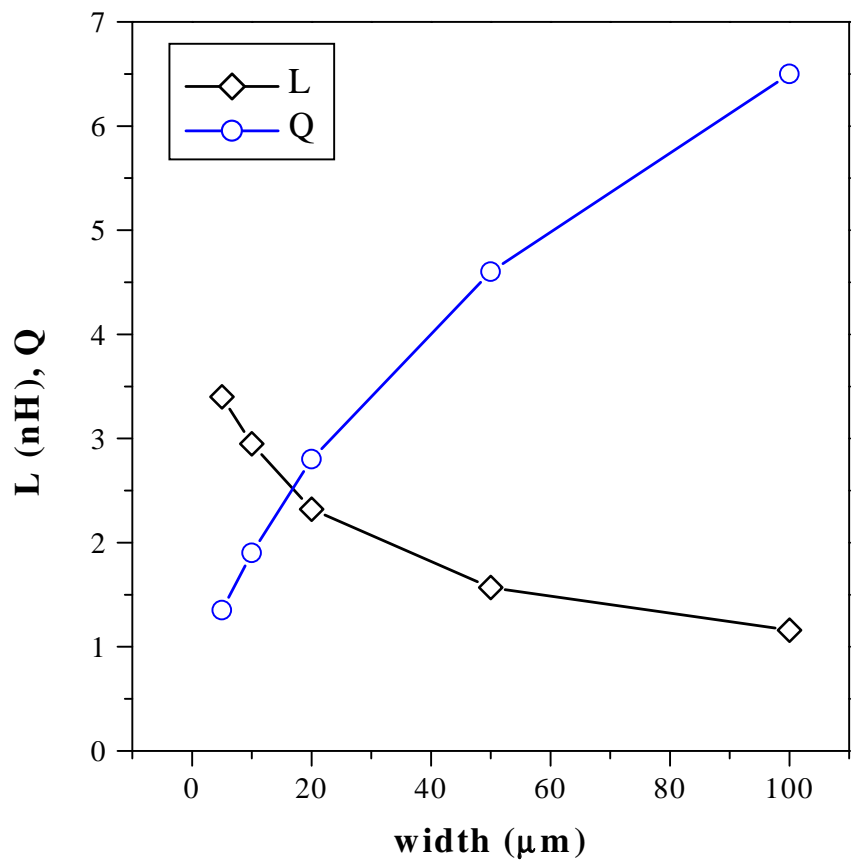


Figure 9: -

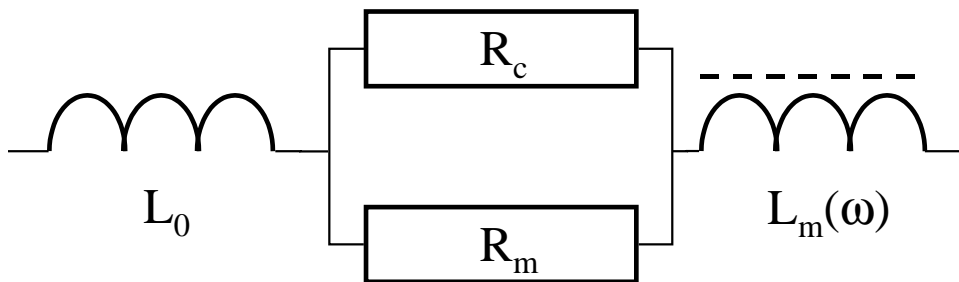


Figure 10: -